Lattice Boltzmann method for modeling liquid-vapor interface configurations in porous media

Michael C. Sukop[1] and Dani Or

Department of Civil and Environmental Engineering, University of Connecticut, Storrs, Connecticut, USA

[1] The lattice Boltzmann method (LBM) has emerged as a powerful tool for simulating the behavior of multiphase fluid systems in complex pore networks. Specifically, the single component multiphase LBM can simulate the interfacial phenomena of surface tension and adsorption and thus be used for modeling fluids such as water and its vapor in porous media. This paper provides an introduction to LBM applications to interface configurations in partially saturated porous media. Key elements of this LBM application are fluid-fluid and fluid-solid interactions that successfully mimic the Young-Laplace equation and liquid film adsorption. LBM simulations of liquid behavior in simple pore geometry considering capillarity and adsorption are in good agreement with analytical solutions and serve as critical first steps toward validating this approach. We demonstrate the usefulness of LBM in constructing virtual liquid retention measurements based on porous media imagery. Results of this study provide a basis for application of LBM to understanding liquid configurations in more complex geometries and clear a path for applications involving interface migration, flow, and transport in partially saturated porous media. *INDEX TERMS:* 1866 Hydrology: Soil moisture; 1875 Hydrology: Unsaturated zone; 3210 Mathematical Geophysics: Modeling; 3230 Mathematical Geophysics: Numerical solutions; *KEYWORDS:* Lattice Boltzmann

Citation: Sukop, M. C., and D. Or (2004), Lattice Boltzmann method for modeling liquid-vapor interface configurations in porous media, *Water Resour. Res.*, *40*, W01509, doi:10.1029/2003WR002333.

1. Introduction

[2] The lattice Boltzmann method has emerged as a powerful tool for simulating fluid behavior in partially saturated porous media that surpasses standard approaches based on the Richards equation and provide insights into phenomena not yet observable with current experimental methods. This study assesses the potential of the single component multiphase LBM for the simulation of liquid film adsorption, capillary condensation, and hysteretic wetting/drying in angular pores and in more complex porous media.

[3] The Boltzmann equation is the foundation of modern gas statistical mechanics. Lattice Boltzmann models simulate a swarm of hypothetical particles that exist on a lattice. A key aspect of the LBM is that permissible velocity directions and magnitudes are constrained to a handful of discrete values on a lattice thereby greatly simplifying solution of the Boltzmann equation. These methods have particular significance for porous media because of the ease of incorporating geometrically complex boundary conditions relative to continuum modeling approaches. Lattice Boltzmann methods also have a remarkable capability to simulate interfaces between different fluids (multicomponent multiphase), or between a liquid and its vapor (single component multi-phase). Interfaces arise, deform, and migrate rather "naturally" without the need for complex interface tracking algorithms. Additionally, the single component multiphase LBM has the distinctive ability to simulate evaporation, condensation, and cavitation phenomena.

[4] Lattice Boltzmann models are descendants of lattice gas cellular automata, which follow the motions of individual particles and were first presented as a viable means of solving the Navier-Stokes equations in the landmark work of Frisch et al. that appeared in 1986. In the most simplistic sense, lattice Boltzmann models work with distributions of particles at each lattice point rather than with individual particles. This has advantages for certain types of simulations in that averaging is not required to obtain smooth velocity fields. *Chen and Doolen* [1998] and *Qian et al.* [1995] prepared reviews of lattice Boltzmann methods for fluid flows, and a number of books are available [*Rothman and Zaleski*, 1997; *Wolf-Gladrow*, 2000; *Succi*, 2001].

[5] The first lattice gas models utilizing long-range particle interactions and therefore capable of simulating phase transitions between liquid and gas appeared in the late 1980s and early 1990s [*Rothman and Keller*, 1988; *Appert and Zaleski*, 1990]. Soon after, the Appert and Zaleski model was applied to soil water phenomena [*Di Pietro et al.*, 1994] and to evaporation in porous media [*Pot et al.*, 1996]. *Di Pietro et al.* [1994] simulated transient unsaturated "water" infiltration between parallel plates, Phillip's infiltration equation, and infiltration into an aggregated medium with a vertical macropore. *Pot et al.* [1996] used a two-dimensional liquid-gas lattice gas model to simulate evaporation in simple capillary channels and in a random

---

[1]Now at Department of Earth Sciences, Florida International University, Miami, Florida, USA.

porous medium. They observed vapor fluxes, appreciable liquid film fluxes, and menisci bursts in a porous medium.

[6] A number of different approaches have been used to derive multiphase LB models and this continues to be an area of rapid development. The earliest models can be classified [*Succi*, 2001] as "chromodynamic". Here particles of different "color" are redistributed to enhance particle color gradients and cause phase separation [*Gunstensen et al.*, 1991]. Pseudopotential models [e.g., *Shan and Chen*, 1994] impose interactions much like van der Waals attractions between fluid particles. Phase separation occurs when the attractive interaction is strong enough and the "temperature" is low enough (subcritical). There are also so-called "free energy" approaches proposed by *Swift et al.* [1996], and "finite density" models that use the Enskog equation for dense gases [*Luo*, 2000; *He and Doolen*, 2002]. Finite density models seem to hold the key to the ultimate development of the LBM for practical applications due to the more realistic and consistent treatment of the equation of state that preserves the essential (molecular) physics of the process. Here we work with the *Shan and Chen* [1993, 1994] model extended for solids interactions. Although this model has numerous shortcomings, it is exceptionally versatile, and problems that have long defied quantitative treatment can now be examined.

[7] Most applications of multiphase lattice gas and LB methods to porous media have focused on assessments of the validity of Darcy's law-based relative permeability concepts for multicomponent oil/water-like systems [*Buckles et al.*, 1994; *Soll et al.* 1994a, 1994b; *Martys and Chen*, 1996; *Langaas and Papazacos*, 2001]. Density contrasts between the fluids are small in these systems and there is no possibility of phase exchange via evaporation or condensation. In contrast, relatively little has been done with multiphase single component simulations, particularly in systems involving solid surfaces. Several researchers [*Angelopoulos et al.*, 1998; *Briant et al.*, 2002] have presented LB simulations of single component multiphase fluids in small model porous media using the "free-energy" lattice Boltzmann model of *Swift et al.* [1996], which differs considerably from the model we use here. It has been criticized as a "top down" approach where macroscopic properties such as the surface tension are prescribed [*Chin et al.*, 2002]. This is in contrast to "bottom up" approach of the *Shan and Chen* [1993, 1994] (henceforth SC) model where such macroscopic properties emerge from the particle scale dynamics. Recent work by *He and Doolen* [2002] suggests that elements of both the SC model used in this paper and the free energy model of *Swift et al.* [1996] are necessary for a complete treatment of the relevant physics. Using a model similar to the one we developed for the work reported here, *Raiskinmäki et al.* [2000] simulated spreading of three-dimensional droplets on smooth and rough surfaces. *Raiskinmäki et al.* [2002] consider the dynamics of capillary rise using the same model. *Sukop and Or* [2003] use the same model applied in this current paper to demonstrate the potential for solving invasion percolation and velocity-dependent (capillary number-dependent) invasion of non-wetting phase (drainage) in porous media.

[8] Despite this progress and the great promise of these models for simulating multiphase and multicomponent flows in complex porous media, little has been done to verify adsorption behavior and interface configurations, particularly for single-component multiphase systems. Here we compare LB simulations of adsorbed films in slits and interface configurations in angular pores with analytical calculations presented by *Tuller et al.* [1999] as first efforts toward verification of single-component multiphase LBM for such phenomena.

[9] This paper is organized as follows: a theoretical section briefly introduces the LBM with emphasis on single component multiphase variants and "adsorption" to solid surfaces. Physicochemical models for adsorption, capillary condensation, and hysteretic wetting and drying of angular pores are introduced in the same section. In the Results section, simulations are compared with the physicochemical models. Discussion and conclusion sections follow.

2. Theoretical Considerations

2.1. Single Component Multiphase LBM

[10] The lattice Boltzmann model follows the evolution of a hypothetical swarm of particles via direction-specific density functions on a lattice. Lattice Boltzmann methods are devised to solve the Boltzmann equation in a velocity space that is reduced to a handful of discrete microscopic velocities. Macroscopic velocities that arise from the summation of these microscopic velocities occupy the entire continuum of directions. With the incorporation of cohesive forces between the particles, spontaneous separation into liquid and gas phases occurs and interfaces form.

[11] The triangular lattice has the simplest structure and played an important historical role in the development of lattice gas methods [*Frisch et al.*, 1986], however many modern LBM are now computed on rectilinear lattices. A classification system for the various discretizations that can be constructed on rectilinear lattices is in widespread use. The popular LB scheme referred to as D2Q9 is two-dimensional and uses 9 velocities; eight are shown in Figure 1a and the ninth is zero (i.e., "rest particles"). In this model, the length scale (1 lattice unit or 1 lu) is fixed by the distance between nodes along the Cartesian coordinate axes (Figure 1a). The velocity magnitude of e_1 through e_4 is 1 lattice unit per time step or 1 lu ts^{-1}, and the velocity magnitude of e_5 through e_8 is $\sqrt{2}$ lu ts^{-1}. (lu, mu, and ts refer to LBM lattice units, mass units, and time step respectively.)

[12] We use the D2Q9 model with single relaxation time. There are also models with direction-dependent relaxation times. Details of all these models are described elsewhere [e.g., *Succi*, 2001; *Wolf-Gladrow*, 2000]. Here we briefly review the basic equations and some unique aspects of multiphase, single-component models.

[13] Lattice Boltzmann calculations proceed in two principal steps. The first is collision where direction-specific density distributions are "relaxed" toward quasi-equilibrium distributions. Then a "streaming" process moves the distributions to neighboring nodes. The lattice Boltzmann equation with streaming and single relaxation time collision operator (commonly referred to as BGK after Bhatnagar-Gross-Krook [*Bhatnagar et al.*, 1954]) is

$$f_a(\mathbf{x} + \mathbf{e_a}\Delta t, t + 1) = f_a(\mathbf{x}, t) - \frac{[f_a(\mathbf{x}, t) - f_a^{eq}(\mathbf{x}, t)]}{\tau} \quad (1)$$
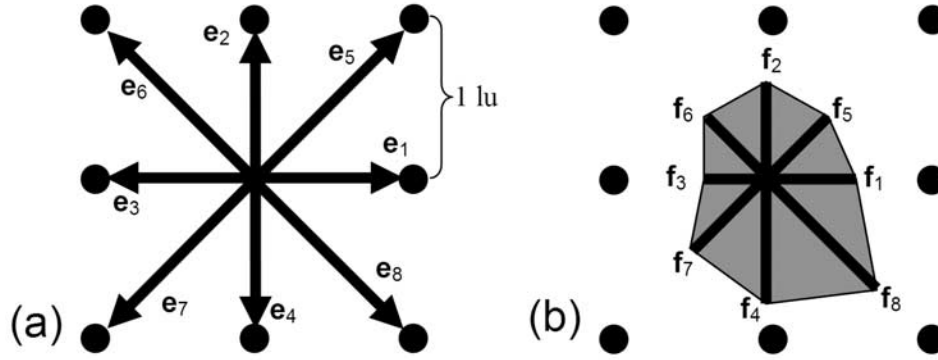
Figure 1. (a) D2Q9 lattice, definition of lattice unit, and discrete velocities; (b) example of direction-specific density distribution function f.

Here $\mathbf{x}$ is a position vector and "a" refers to one of 8 principal directions on the lattice and a = 9 for zero velocity rest particles. $\mathbf{e_a}$ are velocity vectors, t is time, Δt is the time step (taken as 1 ts here), τ is the relaxation time (1 (dimensionless) in this work), f_a is the density of particles in the "a" direction, and f_a^{eq} are the components of the equilibrium distribution function. The f_a and f_a^{eq} can be thought of as a directional histogram of densities (Figure 1b). On the D2Q9 lattice, f_a^{eq} are given by

$$f_a^{eq}(\mathbf{x}) = w_a \rho(\mathbf{x}) \left[1 + 3 \frac{\mathbf{e_a} \bullet \mathbf{u}}{c^2} + \frac{9}{2} \frac{(\mathbf{e_a} \bullet \mathbf{u})^2}{c^4} - \frac{3}{2} \frac{\mathbf{u}^2}{c^2} \right] \quad (2)$$

for a = 1, ... 9. The weights w_a are 4/9 for the rest particles (a = 9), 1/9 for a = 1, 2, 3, 4, and 1/36 for a = 5, 6, 7, 8. The maximum attainable macroscopic speed on the lattice is c (c = 1 lu ts^{-1} in our study). Note however, that the derivation of the lattice Boltzmann equation is based on a small velocity assumption and the practical maximum macroscopic velocity is considerably smaller ($|\mathbf{u}| < \sim 0.1$ c). The density of particles ρ at $\mathbf{x}$ is the sum of the individual directional densities [$\rho(\mathbf{x}) = \Sigma_a f_a(\mathbf{x})$] and the macroscopic velocity $\mathbf{u}$ at $\mathbf{x}$ is $\mathbf{u} = \Sigma_a \mathbf{e_a} f_a(\mathbf{x})/\rho(\mathbf{x})$. Following collision computation in (1), the streaming operation completes momentum transfer by moving the directional distributions to downstream nodes at t + Δt (by simply reassigning spatial subscripts for f_a from $\mathbf{x}$ to $\mathbf{x} + \mathbf{e_a} \Delta t$).

[14] These equations form the basis of the single fluid LBM on the D2Q9 lattice. In general, one begins with some initial distribution f_a at all lattice nodes, then the effects of boundaries and forcing (see below) are incorporated. Finally, the equilibrium distributions are recomputed via (2), and the densities and velocities at the next time step are solved via (1).

2.2. Adsorption in LBM

[15] The preceding discussion pertains to pure fluid systems with no interactions with solid surfaces. Introduction of solid surfaces requires new boundary conditions (see below) and, if adsorption from a vapor phase or preferential wetting is to be simulated, introduction of fluid-solid interaction forces. A force between fluid particles and solid surfaces can be introduced into the LBM formulation as follows [*Martys and Chen*, 1996]:

$$\mathbf{F_{ads}}(\mathbf{x},t) = -G_{ads}\rho(\mathbf{x},t)\sum_{a=1}^{8} w_a s(\mathbf{x}+\mathbf{e_a})\mathbf{e_a} \quad (3)$$

Here G_{ads} is a constant that controls the strength of the fluid-solid interaction, s is an index function that has value 1 if the site at $\mathbf{x} + \mathbf{e_a}$ is a solid and is zero otherwise, w_a are weighting factors equal to 2 for a = 1, 2, 3, 4 and equal to 1 for a = 5, 6, 7, 8. *Martys and Chen* [1996] include this weighting in the context of the D3Q19 (dimension 3, 19 velocities) lattice, and *Raiskinmäki et al.* [2000] first mention the w_a factors for solids interaction. *Shan and Chen* [1993, 1994] worked on an equilateral triangular lattice where the weight constants w_a were unnecessary.

[16] The simulations presented here use a slightly modified version of equation (3) that does not include the density term. Thus the force exerted on any mass occupying a nearest neighbor node adjacent to the surface is a constant. This gives results more in agreement with analytical models discussed in subsequent sections of this article. The details of surface interactions are not fully understood [*Adamson and Gast*, 1997] and this represents a critical area for further LBM research.

[17] To incorporate the solid interaction force (and other forces) into the LBM, we recognize that from Newton's Law $\mathbf{F} = m\mathbf{a} = m\, d\mathbf{u}/dt$, where m is mass. With discrete representation of velocity and relaxation time τ, and using density ρ as mass per unit area basis (due to the two-dimensional nature of the model), we have

$$\Delta \mathbf{u} = \frac{\tau \mathbf{F}}{\rho} \quad (4)$$

Thus equation (4) provides a means for incorporating forces into the model via velocities used in (2) according to $\mathbf{U} = \mathbf{u} + \tau \mathbf{F}_1/\rho + \tau \mathbf{F}_2/\rho + \ldots$, where the subscripts refer to different forces; in particular here we have adsorptive and cohesive (see section 2.3) forces. Other forces, such as gravitational force, can readily be incorporated this way. See, however, the

work of *Luo* [2000] for discussion of some difficulties with this approach.

2.3. Cohesive Force and Liquid-Vapor Model

[18] The principal distinguishing characteristic of the multiphase, single-component LB model is the inclusion of a cohesive force between fluid particles of one particular ''species'' that leads to phase separation. The force is incorporated as follows [*Shan and Chen*, 1993]:

$$\mathbf{F}(\mathbf{x}, t) = -G\psi(\mathbf{x}, t) \sum_{a=1}^{8} w_a \psi(\mathbf{x} + \mathbf{e_a}\Delta t, t)\mathbf{e_a} \qquad (5)$$

where $\mathbf{F}$ is the fluid-fluid interaction force, G is an interaction strength constant that is negative for particle attraction, ψ is a potential function that depends on density (see below), and $\mathbf{e_a}$ are velocity vectors as above, pointing in one of the a = 1, 2,..., 8 velocity directions on the D2Q9 lattice. The weighting factor w_a is 2 for a = 1, 2, 3, 4 and is 1 for a = 5, 6, 7, 8 as above. In essence, with G < 0 for attraction between particles, this force is stronger when the densities are higher leading to a tendency for phase separation and the emergence of surface tension in the LBM. The cohesive force enters the model through velocity adjustment in precisely the way described above for the adsorptive force.

[19] The function ψ can be varied arbitrarily in the SC model framework but must be monotonic and bounded. It relates directly to the attractive force $\mathbf{F}$ (and hence the potential field) between nearest neighbor fluid particles. A particular ψ function is given by *Shan and Chen* [1994]:

$$\psi(\rho) = \psi_0 \exp\left(^{-\rho_0}/_\rho\right) \qquad (6)$$

Parameters that control this ψ function are the constants ψ_0 and ρ_0. This functional form of ψ leads to LB models whose ''...behavior is consistent with that of an isothermal process...'' [*Shan and Chen*, 1994] [see also *He and Doolen*, 2002]. ψ_0 and ρ_0 can be varied arbitrarily. All of the results here use this form of the ψ function. With these basic concepts in place, the dynamics of phase separation and attainment of equilibrium configurations can be simulated.

2.4. Equation of State

[20] The equation of state (EOS) relates the temperature, pressure, and volume (or density) of a fluid. The simplest EOS is that for an ideal gas

$$P = \rho RT, \qquad (7)$$

which is a linear relationship expressing the proportionality between pressure P and density ρ when the temperature is held constant. R is the ''gas constant'' and T is the temperature.

[21] Non-idealities arise from the non-negligible volume of gas molecules (hence gasses become much more difficult to compress as the density increases) and from the attractive interactions between gas molecules (which reduce the pressure). These considerations form the basis of the van der Waals corrections to the ideal gas model. The van der Waals model has been successful in that it captures some of the essential features of liquid/vapor systems. In particular,

for certain (subcritical) temperature ranges the van der Waals model yields a non-monotonic P(ρ) relationship, which admits the possibility that at a single pressure, two densities of the same material can coexist. The low density corresponds to a vapor phase while the high density corresponds to a liquid phase.

[22] The cohesive forces described above lead to an EOS of the form

$$P = \rho RT + k_0 \frac{GRT}{2}[\psi(\rho)]^2 \qquad (8)$$

This has the essential feature of the van der Waals equation (nonmonotonicity at certain T) that allows liquid/vapor phase coexistence. Equation (8) is essentially the form given by *He and Doolen* [2002], except that we include the constant k_0, which we find to have a value of 24 in our simulations. We solve for k_0 by equating $P_l = P_g$ at equilibrium for a flat liquid/vapor interface and rearranging (8) to obtain

$$k_0 = \frac{2\left(\rho_g - \rho_l\right)}{G\left\{[\psi(\rho_l)]^2 - \left[\psi\left(\rho_g\right)\right]^2\right\}} \qquad (9)$$

Then liquid and gas densities ρ_l and ρ_g observed in simulations of a flat interface are used together with the G value to compute k_0.

[23] From gas kinetic theory, the kinetic energy per molecule is given by

$$\frac{1}{2}mc^2 = \frac{3}{2}kT \qquad (10)$$

where m is the particle mass, c is the particle speed, k is the Boltzmann constant, and T is the absolute temperature. In the lattice Boltzmann formulation used here, m and c are set to 1 mass unit (mu) and 1 lattice unit per time step (lu ts^{-1}) respectively. Incorporating these values and using a molar basis for m as in (8) where R = k A with A = Avagadro's number leads to

$$RT = \frac{1}{3} \qquad (11)$$

Hence the simplified form of (8) is

$$P = \frac{\rho}{3} + 4G(\psi(\rho))^2 \qquad (12)$$

Figure 2a shows Equation (12) for a series of G values that result in behavior ranging from supercritical (G = −2, no phase separation) to subcritical (G = − 5). ψ_0 is set at 4 and ρ_0 is set to 200 mu lu^{-2}. The densities have dimensions of mass per unit area for this 2-D model. The critical density and critical G value can be determined by setting dP/dρ = 0 and d^{2}P/dρ^2 = 0 respectively. At subcritical values of G, two densities coexist at a single pressure and the fluid spontaneously separates into gas and liquid phases, provided that in simple simulations the overall density lies in the portion of the EOS where dP/dρ < 0. We use G = −5 in all of the simulations presented in this paper.
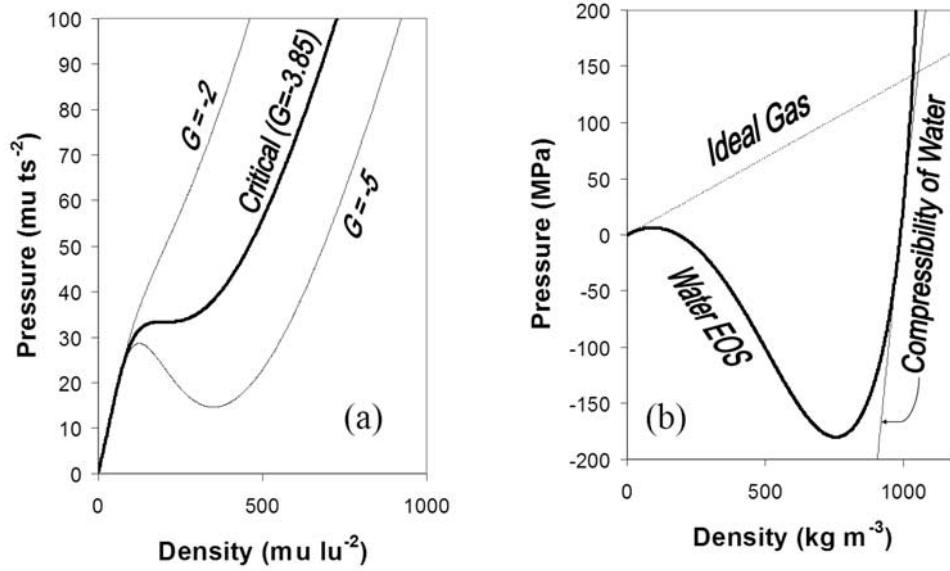
Figure 2. (a) LBM and (b) water equations of state. Water EOS is after *Truskett et al.* [1999].

[24] Figure 2 also provides a comparison between SC-based lattice Boltzmann EOS used in this study (Figure 2a) and the EOS for water (Figure 2b). The near incompressibility of water relative to its vapor is indicated by the relative steepness of the curve in the high and low density regions. In contrast, the liquid compressibility in this lattice Boltzmann EOS is actually greater than the vapor phase compressibility. This is due to the lack of a repulsive potential between particles as the density increases in the SC model; hence the hypothetical particles can closely approach one another. Despite flexibility in the selection of ψ_0 and ρ_0, the fundamental form and hence this characteristic of this EOS is unchanged. Improvement of the EOS is a critical need for advancing single component multiphase LBM simulations and is the subject of intense research [*Luo*, 1998, 2000; *He and Doolen*, 2002]. For the steady state interface configurations that are the focus of this study, however, the EOS described above is adequate.

2.5. Boundary Conditions

[25] Depending on the particular problem being investigated, some combination of boundary conditions is normally employed. These can include periodic or "wrap-around" boundaries (in which for example the last cell in the x direction is taken as adjacent to the first cell in the x direction), closed boundaries (usually just a wall of solids that enforce a "bounce back" boundary), or open boundaries with specified velocity or specified density (equivalent to specified pressure in accordance with the EOS). Implementation of pressure/density boundary conditions in our work follows the approach proposed by *Zou and He* [1997].

[26] In order to implement a model that incorporates collisions with solid objects it is necessary to split the collision and streaming steps that are combined in equation (1). When **x** represents a fluid site, collisions are computed according to

$$f_a(\mathbf{x}, t+1) = f_a(\mathbf{x}, t) - \frac{[f_a(\mathbf{x}, t) - f_a^{eq}(\mathbf{x}, t)]}{\tau} \qquad (13)$$

(i.e., (1) without streaming from **x** to $\mathbf{x} + \mathbf{e_a}\Delta t$). If **x** is a solid site, the simplest approach is to rotate all densities at the site by 180 degrees: for example, $f_1(\mathbf{x}, t+1) = f_3(\mathbf{x}, t)$ or $f_6(\mathbf{x}, t+1) = f_8(\mathbf{x}, t)$. This is the popular "bounce back" boundary condition (Figure 3). According to *Chen et al.* [1996], bounce back works well for $\tau = 1$, but not other τ. τ principally controls the viscosity and hence is not a critical parameter for the static interface configuration simulations we describe here.

[27] After collision via (13) and application of bounce back at the appropriate lattice sites, the streaming step is simply

$$f_a(\mathbf{x} + \mathbf{e_a}\Delta t, t+1) = f_a(\mathbf{x}, t+1) \qquad (14)$$

Implementing boundary and initial conditions remains challenging for a number of reasons. One of the most difficult is the presence of high density gradients in the initial density distribution. This might preclude for example the possibility of setting a vapor boundary directly adjacent to a surface with a liquid film. On the other hand, it appears to be important to begin with liquid films on solid surfaces to avoid the extreme velocities that develop to form such films from a vapor phase, in spite of the presence of high gradients in initial conditions these can imply. Clearly, the destabilizing effect of the adhesive force is significant if it is not satisfied to some extent at the outset. Experience is probably the best guide to workable initial and boundary conditions at this time.

2.6. Numerical Stability

[28] Numerical stability in LBE requires that the speed of a fluid is less than the maximum speed supported by the lattice. This is commonly known as the CFL (Courant, Friedrichs, Lewy) condition and can be written as velocity < c, where c = delta x/delta t = 1 in the present work. We augment the velocity with terms that represent contributions from surface tension and surface interaction forces that can lead to violations of the CFL condition. Also, the value of τ
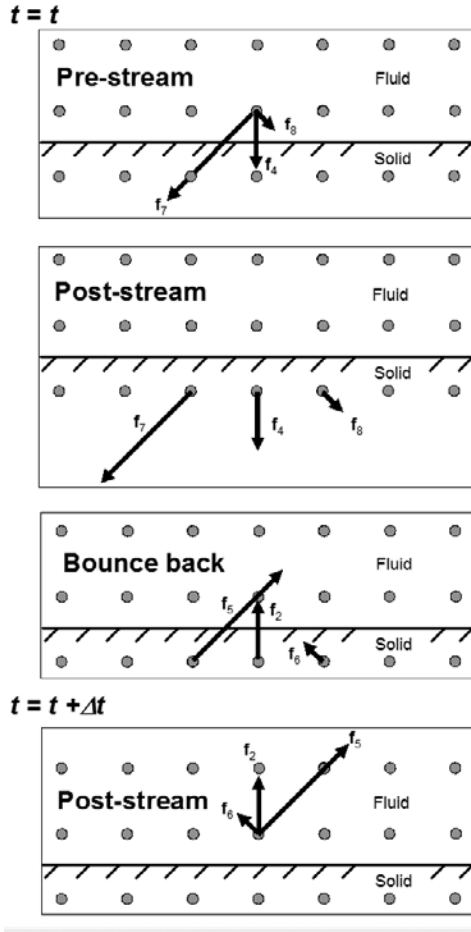
Figure 3. Schematic illustration of bounce back rule for interaction with solids.

must be greater than 1/2. We have been careful to choose initial conditions, boundary conditions, and parameter values that avoid numerical instabilities.

2.7. Physicochemical Models for Adsorption, Capillary Condensation, and Liquids in Angular Pores

[29] The ultimate success of the LBM for simulating liquid-vapor phenomena in porous media depends on its ability to reproduce observed behavior, which for simple geometries is well described by physicochemical models. Here we briefly review physicochemical models for adsorption, capillary condensation, and liquid configurations in angular pores and then compare the predictions of these models with our simulation results.

2.7.1. Adsorption and Capillary Condensation

[30] *Tuller et al.* [1999, and references therein] have pointed out that the formation of liquid films on solid surfaces is a complex process that depends on molecular, electrostatic, structural, and adsorptive forces and thus on surface properties and liquid polarity and solute content. The lattice Boltzmann model does not attempt to specifically simulate each of these processes but makes considerable simplification by including a simple attractive "interaction" with the solid surface.

[31] As a first step here, we follow *Tuller et al.* [1999] and focus on the molecular interactions (i.e., van der Waals

forces) between surfaces and fluids because of their omnipresence and relative importance in water/mineral systems.

[32] Physical adsorption is the process whereby van der Waals forces cause fluid molecules to adhere to a surface. In its simplest form, adsorption occurs from the vapor onto a flat surface. The adsorbed film thickness h is governed by the disjoining pressure Π, which is taken as the difference between the actual vapor pressure and that of the free, flat liquid-vapor interface:

$$h(\Pi) = \sqrt[3]{\frac{A_{svl}}{6\pi\Pi}} \qquad (15)$$

where A_{svl} is the Hamaker constant for the solid/vapor interaction through the liquid. Its numerical value is $A_{svl} = -1.9 \times 10^{-19}$ J (for water on mica).

[33] When adsorbed liquid films form on opposing surfaces (as in a slit), there is the potential for their interaction across the vapor phase. In that case, the equation relating the disjoining pressure to the width of the slit H and the adsorbed film thickness h is [*Tuller et al.*, 1999]

$$\Pi = \frac{A_{svl}}{6\pi h^3} - \frac{A_{llv}}{6\pi(H-2h)^3} + \frac{A_{svl}}{6\pi(H-h)^3} \qquad (16)$$

Here A_{llv} is the Hamaker constant for the liquid/liquid interaction through the vapor. It has a value of $A_{llv} = 3.7 \times 10^{-20}$ J (a theoretical value for water).

[34] Capillary condensation [*Tuller et al.*, 1999; *Evans et al.*, 1986] is the phenomenon whereby such opposing adsorbed liquid films coalesce. This when $\partial\Pi/\partial h = 0$ from (16) or at a critical film thickness equal to approximately one-third of the separation distance between two flat surfaces is reached. *Evans et al.* [1986] presented a thorough evaluation of capillary condensation from a chemical physics perspective. *Truskett et al.* [2001] have also considered the thermodynamic implications of the confinement of water between planar surfaces.

[35] The relative saturation of a slit, S, can be expressed as 2h/H. With this relation, we can compute the relative saturation/pressure constitutive relationship for the slit. Such water retention curves provide critical parameterization of partially saturated zone materials. The Results section presents LBM simulations of adsorption and capillary condensation phenomena.

2.7.2. Liquid Configurations in Angular Pores

[36] *Tuller et al.* [1999] demonstrated a means of calculating the water-filled cross-sectional area (Aw_t) in angular pores using the following equation:

$$Aw_t = r^2 F(\gamma) \qquad (17)$$

where r is the radius of curvature of the liquid-vapor interface, which depends on the capillary pressure and is given by the Young-Laplace equation:

$$p_c = \frac{\sigma}{r} \qquad (18)$$

where p_c is the capillary pressure, σ is the surface tension of the liquid (for water 0.0727 J m^{-2} at 20°C), and a zero contact angle is assumed.

[37] $F(\gamma)$ is a shape factor that depends on pore angularity. It is given by

$$F(\gamma) = \sum_{i=1}^{n} \left(\frac{1}{\tan\left(\frac{\gamma_i}{2}\right)} - \frac{\pi(180 - \gamma_i)}{360} \right) \qquad (19)$$

where n is the number of corners and γ_i is the interior angle of corner i. As an example, for a square capillary, $\gamma_i = 90°$ for all n = 4 interior angles. Then $\tan(\gamma_i/2)$ is 1 and $F(\gamma) = 4(1 - \pi/4)$ or 0.8584.

[38] For a pore with cross-sectional area A, the relative saturation is obviously $S = Aw_t/A$. Equations (17), (18), and (19) can be used to compute the high water tension portion of the retention curve that will be followed as water recedes into the pore corners.

[39] Tuller et al. also give the following equation for the radius of curvature at "snap-off imbibition" where the liquid-vapor interface radius of curvature equals the radius of the smallest inscribed circle in the angular pore and the pore spontaneously fills with fluid:

$$r_{imb} = \frac{2A}{P} \qquad (20)$$

where P is the pore's perimeter. For the square capillary example we consider here, $A = (P/4)^2$ and hence $r_{imb} = P/8$ or exactly 1/2 the side length.

[40] To initiate drainage, considerably higher liquid tension must be applied to the capillary. The radius of curvature is given by [*Tuller et al.*, 1999]:

$$r_d = \frac{P}{2\big[(F(\gamma) + \pi) + \sqrt{\pi(F(\gamma) + \pi)}\big]} \qquad (21)$$

We can compute the hysteretic wetting/drying curve for an angular capillary by computing $F(\gamma)$, r_{imb}, and r_d and using the relative saturation $S = Aw_t/A$. If we begin at high liquid tension, where the pore is nearly empty, and then decrease the tension, water will be taken up by the capillary according to

$$S = \frac{\left(\sigma/p_c\right)^2 F(\gamma)}{A} \qquad (22)$$

which is a combination and rearrangement of (17) and (18). Solving (22) for p_c yields

$$p_c = \sigma\sqrt{\frac{F(\gamma)}{AS}} \qquad (23)$$

The uptake of liquid with decreasing tension continues until the snap-off imbibition radius r_{imb} is reached. This radius can be calculated from (20) and the pressure can be calculated with (18). Then the pore fills. Increasing the tension to the level associated with r_d required for drainage causes rapid drainage until the water content reaches the value determined by (21) and (22).

[41] This behavior is expected when the thickness of the adsorbed film on the capillary walls is negligible. When this is not the case, *Tuller et al.* [1999] showed that a "shifted"
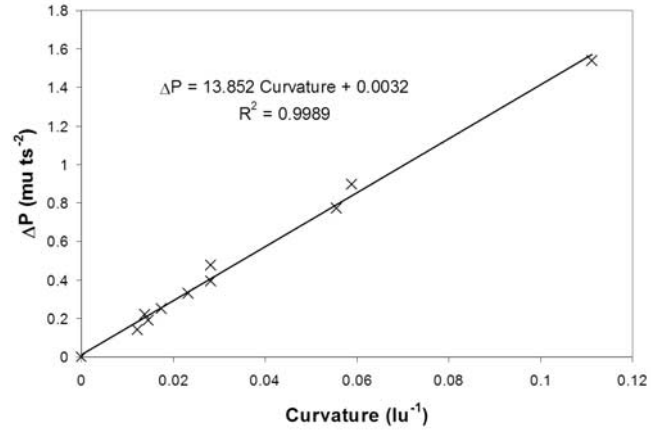
Figure 4. Estimation of surface tension from curvature (1/radius) and pressure difference between inside and outside of simulated drops and bubbles.

Young-Laplace equation, in which the interface is simply shifted away from the wall by the expected film thickness under the imposed tension, gave a reasonable approximation for computing the saturation/tension relationship.

[42] The understanding of the behavior of water in slits and angular pores embodied in these physicochemical models provide excellent fundamental tests of the lattice Boltzmann model's ability to simulate fluid behavior in porous media. We present LBM simulations of these phenomena in the next section.

3. Results

3.1. Tests of the Lattice Boltzmann Model

[43] Next we present a series of simulations that illustrate the LBM's ability to model fluid-fluid interaction leading to surface tension, interactions of liquid/surface pairs leading to variable wetting characteristics, adsorption from a vapor phase, capillary condensation, and hysteretic wetting/drying in angular pores. We compare the LBM results to the analytical models presented in the preceding section. Finally, we show an application to a complex pore network derived from imagery of a natural porous medium.

3.2. Surface Tension

[44] Simulations of phase separation in fully periodic domains using different initial conditions (i.e., different starting mass) result in different final drop and bubble radii. These results provide the information necessary for the determination of surface tension. The Laplace equation relates the radii of the drops and bubbles to the pressure difference between the inside and outside of the drop or bubble:

$$\Delta P = \frac{\sigma}{r} \qquad (24)$$

where ΔP is the pressure difference, r is the radius, and σ is the surface tension.

[45] Simulation results are presented in Figure 4 where the slope of the relationship is the surface tension of the liquid-vapor interface. Ultimately, the surface tension depends on the inter-particle cohesive force, and for the particular EOS

Figure 5. Varying wettability as a function of G_{ads}. (a) $G_{ads} = -15$; (b) $G_{ads} = -25$.

and parameters we use ($G = -5$, $\psi_0 = 4$ and $\rho_0 = 200$), we find the 2-D surface tension $\sigma = 13.85$ lu mu ts^{-2}.

3.3. Wetting

[46] Adjusting the adhesive force constant G_{ads} controls the degree of wetting in LB simulations as illustrated in Figure 5. A partial liquid drop of radius 25 lu is placed adjacent to the bottom solid wall of a 200×200 lu box where the solid surface is at 0 through 45 lu in the y direction. Periodic boundaries are applied on all sides of the computational domain. The simulations are run to near steady state with G_{ads} values of -15 and -25. Reducing G_{ads} from -15 (Figure 5a) to -25 results in a smaller contact angle (Figure 5b). With $G_{ads} = 0$, i.e., no attractive force, non-wetting liquid can be simulated.

[47] High values of Gads lead to compression of the liquid near surfaces causing anomalously high liquid densities. The G_{ads} value of -37 was selected for use in all subsequent simulations to give a zero contact angle and minimize any density anomalies on the surfaces; this value, together with $G = -5$ for the liquid cohesion and the particular EOS parameters, leads to an approximately uniform density from the surface into the bulk liquid. It also results in perfect wetting of the surface; a drop is redistributed on the wall forming a uniform film. G_{ads} could readily be made a function of space and/or time to simulate variable wettability in porous media.

3.4. Adsorption

[48] The upper left inset of Figure 6 shows simulations of steady state adsorbed films in a slit as a function of imposed vapor pressure. The initial condition is a uniform vapor phase inside the slit and a 1 lu liquid film on the solid walls. Equal constant pressure boundaries are applied at the ends of the slit (only the central portions of the slit where two-dimensional effects are negligible are shown). The applied pressures are indicated on Figure 6. The films thicken in accordance with the analytical model presented previously (15) and the simulations can be used to estimate the Hamaker constant A_{svl} for the LBM model (see below).
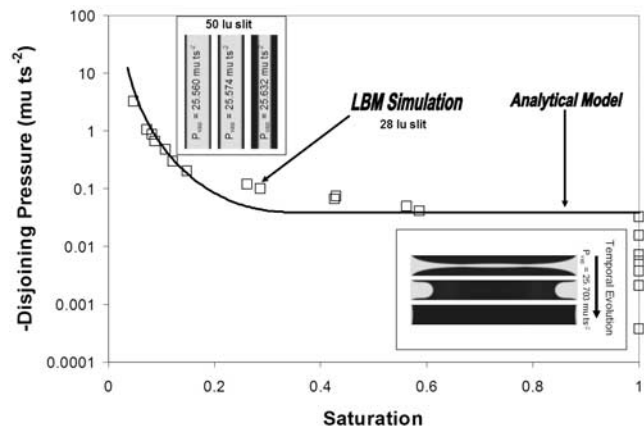
3.5. Capillary Condensation

[49] The bottom right inset of Figure 6 shows a LB simulation of capillary condensation in a slit. The boundary and initial conditions are the same as those used to simulate adsorption, except that the vapor pressure is high enough that films of adequate thickness form on the walls of the slit, liquid bridges form, and the separate films coalesce. This is in agreement with observations and theoretical predictions. As for adsorption above, the capillary conden-

sation simulations can be used to estimate the Hamaker constants (see below).

3.6. Liquid Retention in Slits

[50] Combining the adsorption and capillary condensation phenomena allows the liquid retention characteristics of a slit to be determined. Simulations were conducted over a range of disjoining pressures in order to compute the liquid retention curve for a 28 lu slit (Figure 6). Under dry conditions (more negative disjoining pressure) the density of the adsorbed liquid films decreased considerably, presumably due to the significant compressibility of the liquid phase. Thus the liquid film mass was determined by numerically integrating (trapezoidal rule) the densities adjacent to the wall and to the point at which the density was within 5% of the vapor density. In order to estimate the film thickness, the total film mass was divided by the liquid density associated with a free, flat liquid-vapor interface.

[51] The simulated characteristic curve for the slit corresponds qualitatively to theory (equations (15) and (16)). We estimated the Hamaker constants A_{llv} and A_{svl} by fitting the simulation results to (15) (where only A_{svl} was estimated for films up to 2.66 lu in a 39 lu slit - i.e., the films were assumed to be non-interacting) and to (16) (where A_{llv} and A_{svl} were estimated simultaneously based on films up to 8.2 lu in a 28 lu slit). The independent estimates of A_{svl} were very similar (-26 and -29 lu^3 mu ts^{-2}). A_{llv} was estimated to be 2940 lu^3 mu ts^{-2}. These estimates result in the theoretical curve shown in Figure 6 and could readily be used to make predictions for other conditions. Deviations from the analytical form of the relationship could be the

**Figure 6.** Film adsorption, capillary condensation, and pressure-saturation curve for slit.

result of the mass integration method used to estimate the film thickness, uncertainties about the appropriate disjoining pressure, boundary effects, or lack of complete equilibration in the simulations.

3.7. Simulations in Angular Pores

[52] A fundamental problem with traditional approaches to the behavior of fluids in partially saturated porous media is reliance on the capillary bundle model, in which pores are assumed to have circular cross sections. This type of capillary can be either completely full (when the tension is less than the tension calculated with the Young-Laplace equation from the capillary radius) or completely empty. Cylindrical pore shape is unrealistic for most porous media and the implications for water retention are significant because a substantial fraction of water is held in crevices and corners associated with angular pores. We conducted simulations in two-dimensional angular pores; to control the pressure in such a pore via a domain boundary pressure, the pore must be open to an atmosphere in which the pressure is controlled. In order to investigate liquid retention in a square pore, we conduct simulations on an open rectangular pore and consider saturation in the half square at the closed end. It is desirable to simulate the pore filling and emptying processes by stepping through the pressures as would be done in a typical measurement procedure. Hysteresis expected from the physicochemical model could then be simulated directly.

[53] In Figure 7 we plot pore saturation versus (negative) disjoining pressure. The pore and its liquid menisci at various pressures are also shown. We use an indicator variable to indicate the presence of liquid or vapor at each node in the pore. The criteria are $\rho > \rho_l - (\rho_l - \rho_v)/2$ is liquid (indicator = 1) and $\rho \leq \rho_l - (\rho_l - \rho_v)/2$ is vapor (indicator = 0). The saturation is the sum of the indicator variable inside the half square pore at the closed end of the rectangular pore divided by the total number of nodes in the same region. We observe a clear hysteresis with filling occurring at a disjoining pressure of -0.29 mu ts^{-2} and the initiation of drainage requiring a disjoining pressure of -0.57 mu ts^{-2}.

[54] A significant difference from the capillarity-only case shown by *Tuller et al.* [1999] is the saturation at which filling occurs; in the capillarity-only case it is assumed that
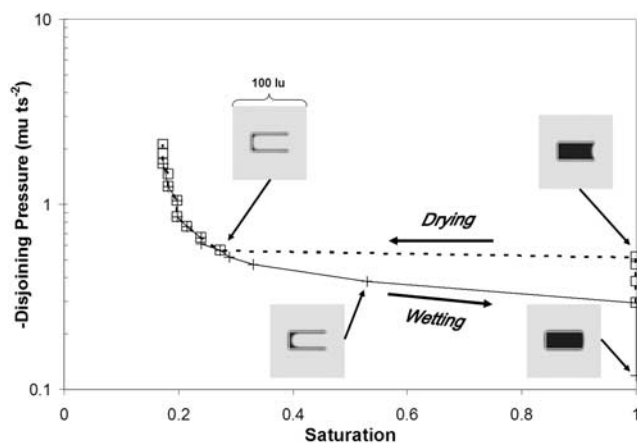
Figure 7. Hysteretic liquid retention curve for "square" pore.
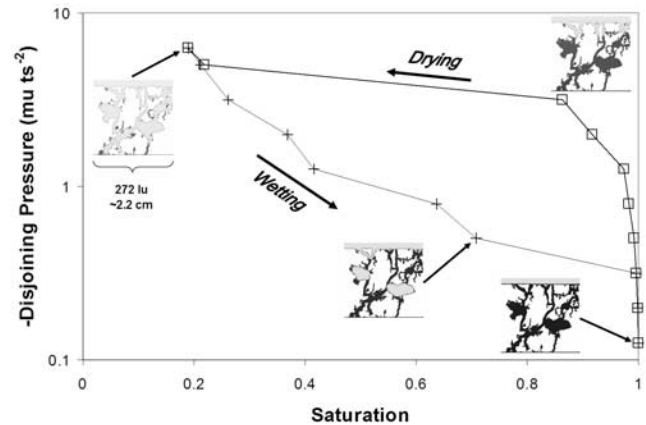
Figure 8. Computed pressure-saturation curve for complex porous medium.

there is no wetting film. The simulation has an appreciable wetting film, which leads to a much higher liquid saturation just prior to filling (0.53 versus 0.21 in the ideal case).

3.8. Complex Pore Network

[55] In the following we illustrate an application of this method for computing water retention in complex porous media as shown on the insets of Figure 8, which are based on two-dimensional imagery of a real soil [*Ringrose-Voase*, 1987]. Vapor and liquid boundaries of equal pressure were applied to the top and bottom of the domain respectively in steps corresponding to equal increments of log(disjoining pressure). Each pressure step was terminated when the relative change in fluid mass in the domain was less that 10^{-7} (measurements on real systems depend on a similar criterion that is generally not well established or quantified). The simulated liquid behavior and characteristic curve show appreciable differences in the fluid configurations during wetting and drying with significant hysteresis.

[56] In traditional measurements at low tensions, the upper boundary is usually open to atmospheric pressure, though efforts to reduce or eliminate evaporation are typically employed. This would allow the head space vapor pressure to equilibrate with the liquid pressure and thus corresponds relatively closely to the process we simulate. A principal difference however is that, because of the relatively high density of the vapor phase in our simulations, significantly more evaporation from and condensation on liquid-vapor interfaces in vapor contact with the vapor boundary is possible than would be expected in water-water vapor systems for example. For higher tensions, measurements typically entail application of gas pressure higher than atmospheric, which forces liquid from a sample through a saturated plate. There are some fundamental differences in these approaches [*Or and Tuller*, 2002] and creative use of LBM simulations would allow the investigation of such different boundary conditions. LBM could also be used to investigate effects of varying practical "equilibrium" criteria on resulting retention curves.

4. Discussion

[57] The results presented here represent preliminary steps in the application of single component multiphase

lattice Boltzmann methods to adsorptive and capillary behavior of fluids in partially saturated porous media. Our goal was to establish the single component multiphase lattice Boltzmann method as a viable approach for the computation of liquid-vapor interface configurations in simple angular 2-D pores and to demonstrate the potential for computing liquid retention behavior from porous media imagery. We demonstrated the LBM's capability for reproducing capillary and adsorptive phenomena that operate in partially saturated porous media, the hysteretic wetting and drying expected and observed in angular pores, and liquid retention curves for more complex porous media derived from imagery.

[58] There are known shortcomings of the method as implemented here; in particular, the EOS employed results in a liquid phase that is more compressible than the gas phase. Also, the density contrast between the liquid and vapor phases is small ($\rho_l/\rho_v \sim 10$) relative to that of water and its vapor. Additionally, the viscosity of the simulated liquid is considerably higher than the viscosity of water and "spurious" velocities exist in the interfaces [*Chen and Doolen*, 1998; *Raiskinmäki et al.*, 2000]. Fortunately, these issues have no implications for the geometry of the steady state interface configurations computed here. As noted above in relation to the liquid retention in a complex medium, the approach to equilibrium may proceed by different means owing to the limited density contrast between liquid and vapor. Similarly, this model's shortcomings are likely to be important for simulations involving dynamic fluid behavior. These issues are at the center of intense research on incorporation of proper equations of state.

[59] The LBM's ability to simulate interfaces, evaporation, condensation, and cavitation are particularly significant for behavior of water in porous media; liquid-vapor equilibria can be attained throughout a connected network by vapor flow, evaporation, and condensation. In contrast to single-component LBM, multicomponent multiphase LBM require phase continuity to attain similar equilibria. For example, a "trapped" non-wetting phase in multicomponent simulations will remain trapped irrespective of the wetting phase potential. In contrast, in single component simulations increasing the wetting phase potential will lead to condensation and the reduction/disappearance of vapor bubbles. While this is advantageous for accurate simulation of certain phenomena, elements of both the multicomponent and single component approaches would be necessary for complete treatment of partially saturated phenomena in porous media in the environment. In reality, in environmental systems a non-wetting air phase consisting mostly of Nitrogen gas contains the water vapor in equilibrium with liquid water surfaces. Finally, single component, multiphase LBM are also capable of simulating liquid cavitation. Recent work [*Or and Tuller*, 2002] suggests that this might be significant in porous media under certain conditions.

[60] Computational issues are likely to increase in importance as the range of scales widens and fully 3-D simulations are implemented. Algorithm optimization and parallelization and careful memory management will be required. In future work, we plan to focus on diffusion processes in partially saturated porous media,

and on hydrodynamics including unstable and intermittent flows.

5. Conclusions

[61] We have demonstrated the ability of single-component multiphase LBM to simulate liquid film adsorption, capillary condensation, hysteretic liquid retention in angular pores, and liquid retention in a complex pore network. LBM simulations were in good agreement with established analytical models for liquid and vapor behavior in slits and simple angular pores, and inspire confidence in the application of LBM to more complex phenomena and larger pore and fracture networks. The LBM has exceptional potential as a numerical experimental platform for the study of long standing issues related to equilibrium in liquid retention measurements, static versus dynamic retention curves, the role of measurement boundary conditions, and the potential for liquid phase cavitation in porous media under tension. We emphasize that detailed simulation of water and its vapor will require the incorporation of an EOS more faithful to the water EOS; fully three-dimensional simulations will be necessary for simulation of realistic pore spaces because of limited connectivity in two dimensions.

[62] Preliminary studies [*Sukop and Or*, 2003] that consider dynamic flow regimes within the LBM framework have shown great promise (and significant challenges). Simultaneous liquid and vapor flow including phase exchange, variable wettability, gravity and buoyancy effects, and flows at relatively high Reynolds number in arbitrarily complex geometry can all be readily simulated by the single component multiphase LBM model used in this study. Furthermore, LBM provides insights into unstable and intermittent flows and interface routing in partially saturated pore networks that cannot be treated by standard continuum approaches such as the Richards equation.

References

Adamson, A. W., and A. P. Gast (1997), *Physical Chemistry of Surfaces*, 6th ed., John Wiley, Hoboken, N. J.

Angelopoulos, A. D., V. N. Paunov, V. N. Burganos, and A. C. Payatakes (1998), Lattice Boltzmann simulation of nonideal vapor-liquid flow in porous media, *Phys. Rev. E*, 57, 3237–3245.

Appert, C., and S. Zaleski (1990), Lattice gas with a liquid-gas transition, *Phy. Rev. Lett.*, 64, 1–4.

Bhatnagar, P. L., E. P. Gross, and M. Krook (1954), A model for collision processes in gases. I. Small amplitude processes in charged and neutral one-component systems, *Phys. Rev.*, 94(3), 511–525.

Briant, A. J., P. Papatzacos, and J. Y. Yeomans (2002), Lattice Boltzmann simulations of contact line motion in a liquid-gas system, *Philos. Trans. R. Soc. London*, 360, 485–495.

Buckles, J. J., R. D. Hazlett, S. Chen, K. G. Eggert, and W. E. Soll (1994), Toward improved prediction of reservoir flow performance, *Los Alamos Sci.*, 22, 112–121.

Chen, S., and G. D. Doolen (1998), Lattice Boltzmann method for fluid flows, *Annu. Rev. Fluid Mech.*, 30, 329–364.

Chen, S., D. Martínez, and R. Mei (1996), On boundary conditions in lattice Boltzmann methods, *Phys. Fluids*, 8, 2527–2536.

Chin, J., E. S. Boek, and P. V. Coveney (2002), Lattice Boltzmann simulation of the flow of binary immiscible fluids with different viscosities

using the Shan-Chen microscopic interaction model, *Philos. Trans. R. Soc. London*, 360, 547–558.

Di Pietro, L. B., A. Melayah, and S. Zaleski (1994), Modeling water infiltration in unsaturated porous media by interacting lattice gas-cellular automata, *Water Resour. Res.*, 30, 2785–2792.

Evans, R., U. Marini Bettolo Marconi, and P. Tarazona (1986), Fluids in narrow pores: Adsorption, capillary condensation, and critical points, *J. Chem. Phys.*, 84, 2376–2399.

Frisch, U., B. Hasslacher, and Y. Pomeau (1986), Lattice-gas automata for the Navier-Stokes equation, *Phys. Rev. Lett.*, 56, 1505–1508.

Gunstensen, A. K., D. H. Rothman, S. Zaleski, and G. Zanetti (1991), Lattice Boltzmann model of immiscible fluids, *Phys. Rev. A*, 43, 4320–4327.

He, X., and G. D. Doolen (2002), Thermodynamic foundations of kinetic theory and lattice Boltzmann models for multiphase flows, *J. Stat. Phys.*, 107, 309–328.

Langaas, K., and P. Papazacos (2001), Numerical investigations of the steady state relative permeability of a simplified porous medium, *Transp. Porous Media*, 45, 241–266.

Luo, L.-S. (1998), Unified theory of lattice Boltzmann models for nonideal gases, *Phys. Rev. Lett.*, 81, 1618–1621.

Luo, L.-S. (2000), Theory of the lattice Boltzmann method: Lattice Boltzmann models for non-ideal gases, *Phys. Rev. E*, 62, 4982–4996.

Martys, N. S., and H. Chen (1996), Simulation of multicomponent fluids in complex three-dimensional geometries by the lattice Boltzmann method, *Phys. Rev. E*, 53, 743–750.

Or, D., and M. Tuller (2002), Cavitation during desaturation of porous media under tension, *Water Resour. Res.*, 38(5), 1061, doi:10.1029/2001WR000282.

Pot, V., C. Appert, A. Melayah, D. H. Rothman, and S. Zaleski (1996), Interacting lattice gas automaton study of liquid-gas properties in porous media, *J. Phys. II Fr.*, 6, 1517–1534.

Qian, Y. H., S. Succi, and S. A. Orszag (1995), Recent advances in lattice Boltzmann computing, *Annu. Rev. Comput. Phys.*, 30, 195–242.

Raiskinmäki, P., A. Koponen, J. Merikoski, and J. Timonen (2000), Spreading dynamics of three-dimensional droplets by the lattice Boltzmann method, *Comput. Math. Sci.*, 18, 7–12.

Raiskinmäki, P., A. Shakib-Manesh, A. Jäsberg, A. Koponen, J. Merikoski, and J. Timonen (2002), Lattice-Boltzmann simulations of capillary rise dynamics, *J. Stat. Phys.*, 107, 143–157.

Ringrose-Voase, A. J. (1987), A scheme for the quantitative description of soil macrostructure by image analysis, *J. Soil Sci.*, 38, 343–356.

Rothman, D. H., and J. M. Keller (1988), Immiscible cellular-automaton fluids, *J. Stat. Phys.*, 52, 1119–1127.

Rothman, D. H., and S. Zaleski (1997), *Lattice-Gas Cellular Automata*, Cambridge Univ. Press, New York.

Shan, X., and H. Chen (1993), Lattice Boltzmann model for simulating flows with multiple phases and components, *Phys. Rev. E*, 47, 1815–1819.

Shan, X., and H. Chen (1994), Simulation of nonideal gases and liquid-gas phase transitions by the lattice Boltzmann equation, *Phys. Rev. E*, 49, 2941–2948.

Soll, W. E., K. E. Eggert, D. W. Grunau. and A. L. Schafer-Perini (1994a), A study of multiphase flow in fractured porous media using a microscale lattice Boltzmann approach, in *Computational Methods in Water Resources X*, pp. 693–700, Kluwer Acad., Norwell, Mass.

Soll, W. E., S. Y. Chen, K. G. Eggert, D. W. Grunau, and D. R. Janecky (1994b), Application of the lattice Boltzmann/lattice gas technique to multi-fluid flow in porous media, in *Computational Methods in Water Resources X*, pp. 991–999, Kluwer Acad., Norwell, Mass.

Succi, S. (2001), *The Lattice Boltzmann Equation for Fluid Dynamics and Beyond*, Clarendon, Oxford, U. K.

Sukop, M. C., and D. Or (2003), Invasion percolation of single-component, multiphase fluids with lattice Boltzmann models, *Physica B*, 338, 298–303.

Swift, M. R., E. Orlandini, W. R. Osborn, and J. M. Yeomans (1996), Lattice Boltzmann simulations of liquid-gas and binary fluid systems, *Phys. Rev. E*, 54, 5041–5052.

Truskett, T. M., P. D. Debenedetti, S. Sastry, and S. Torquato (1999), A single-bond approach to orientation-dependent interactions and its implications for liquid water, *J. Chem. Phys.*, 111, 2647–2656.

Truskett, T. M., P. D. Debenedetti, and S. Torquato (2001), Thermodynamic implications of confinement for a water-like fluid, *J. Chem. Phys.*, 114, 2401–2418.

Tuller, M., D. Or, and L. M. Dudley (1999), Adsorption and capillary condensation in porous media: Liquid retention and interfacial configurations in angular pores, *Water Resour. Res.*, 35, 1949–1964.

Wolf-Gladrow, D. A. (2000), *Lattice-Gas Cellular Automata and Lattice Boltzmann Models: An Introduction*, Lect. Notes Math., 1725.

Zou, Q., and X. He (1997), On pressure and velocity boundary conditions for the lattice Boltzmann BGK model, *Phys. Fluids*, 9, 1591–1598.

D. Or, Department of Civil and Environmental Engineering, University of Connecticut, 261 Glenbrook Road Unit 2037, Storrs, CT 06269-2037, USA.

M. C. Sukop, Department of Earth Sciences, Florida International University, University Park, PC 344, 11200 SW 8th Street, Miami, FL 33199, USA. (sukopm@fiu.edu)